PHYSICAL REVIEW FLUIDS **3**, 062001(R) (2018)

Rapid Communications | Editors' Suggestion

Wall slip of complex fluids: Interfacial friction versus slip length

Benjamin Cross, Chloé Barraud, and Cyril Picard
Université Grenoble Alpes, CNRS, LIPhy, F-38000 Grenoble, France

Liliane Léger and Frédéric Restagno
Laboratoire de Physique des Solides, CNRS, Université Paris-Sud, Université Paris-Saclay, 91405 Orsay Cedex, France

Élisabeth Charlaix*
Université Grenoble Alpes, CNRS, LIPhy, F-38000 Grenoble, France

(Received 21 February 2018; published 15 June 2018)

Using a dynamic surface force apparatus (SFA), we demonstrate that the notion of slip length used to describe the boundary flow of simple liquids is not appropriate for viscoelastic liquids. Rather, the appropriate description lies in the original Navier's partial slip boundary condition, formulated in terms of an interfacial friction coefficient. We establish an exact analytical expression to extract the interfacial friction coefficient from oscillatory drainage forces between a sphere and a plane, suitable for dynamic SFA or atomic force microscopy noncontact measurements. We use this model to investigate the boundary friction of viscoelastic polymer solutions over 5 decades of film thicknesses and 1 decade in frequency. The proper use of the original Navier's condition describes accurately the complex hydrodynamic force up to scales of tens of micrometers, with a simple Newtonian-like friction coefficient that is not frequency dependent and does reflect closely the dynamics of an interfacial depletion layer at the solution-solid interface.

DOI: 10.1103/PhysRevFluids.3.062001

Flows of complex liquids are familiar and useful. Unlike Newtonian fluids, they display complex bulk rheological behavior, nonlinear and frequency dependent, but the way they flow also involves their boundary conditions on solid surfaces. The boundary condition (b.c.) is relevant not only for small-scale flows, occurring, for instance, in biomedical applications, microfluidic devices, food and oil engineering, but also for the faithful characterization of the bulk rheology [1–5].

As in the case of simple liquids, the slippage of complex fluids at walls is commonly characterized by a slip length b, defined by the ratio of the fluid velocity at the solid surface to the shear rate at the wall: $v_{\text{slip}} = b\partial v(z)/\partial z$, with z the direction normal to the boundary. But the notion of slip length, now well established and understood in the case of simple fluid flowing on various types of solid surfaces [6–12] or Newtonian polymer melts [4,13], is far from obvious in the case of more complex fluids. We show here experimentally that the appropriate quantity to describe the boundary slippage of complex fluids without ambiguity is not a slip length but rather a liquid-wall friction coefficient, as originally stated by Navier [14].

We demonstrate this on the particular example of semidilute, viscoelastic polyelectrolyte solutions. Water-soluble polyelectrolytes of high molecular weight are commonly used to thicken water solutions at an affordable price, as small concentrations are sufficient to increase significantly the

*Elisabeth.Charlaix@univ-grenoble-alpes.fr

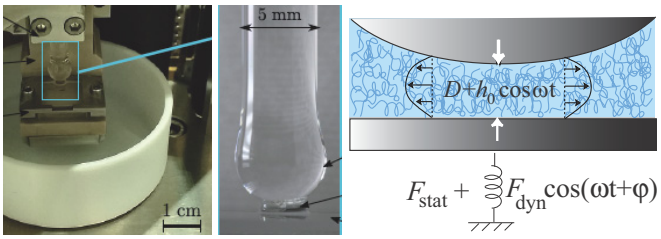

FIG. 1. The dynamic surface force apparatus. Left: Large view of the sphere-plane contact. Center: Detailed view of the contact. Right: Schematic of the flow.

viscosity of the solution [15]. Water-soluble polyelectrolytes of high molecular weight have been reported to display large slip on various types of solid surfaces [16–19]. This large slip has been attributed to the presence of a depletion layer at the solution-solid interface; i.e., a layer with a lower concentration of polymer or even with pure solvent, whose viscosity is significantly lower than that of the solution and induces an apparent slip boundary condition [1,20–23].

Here we use partially hydrolyzed polyacrylamide (HPAM) semidilute solutions, in conditions which were otherwise well characterized by other groups and are industrially used for enhanced oil recovery or water purification [19] (SNF Flopaam 3630S, molecular weight 20.10^6 g/mol solved in deionized water at concentration from 0.8 to 1.6 g/L). The boundary flow of these solutions is studied with a dynamic surface force apparatus (dSFA [24,25]) by confining them between a Pyrex sphere (radius $R = 3.3$ mm) and a Pyrex plane of very low roughness (2 Å rms as measured by AFM). The setup covers sphere-plane distances D ranging over 5 orders of magnitudes from 0.1 nm to 15 μm, allowing one to bridge the macroscopic flow behavior of the liquid to its interfacial hydrodynamics.

The sphere is driven normally to the plane at a low drift velocity $\dot{D}/D < 10^{-2}$ s^{-1} (see Fig. 1). An oscillatory motion of small amplitude ($h_0/D < 10^{-2}$) at angular frequency ω is added to the slow drift motion. The relative sphere-plane displacement as well as the force acting on the plane are measured by two independent external interferometric sensors. From these measurements, we get the steady-state sphere-plane distance D and interaction force F_{stat}, the dynamic amplitude h_0 of the sphere-plane oscillatory displacement which is chosen as the phase origin, the dynamic amplitude F_{dyn} and phase shift φ of the oscillatory interaction force at the frequency ω, and finally the linear force response or mechanical impedance, defined as

$$\tilde{Z}(D,\omega) = \frac{F_{\text{dyn}} e^{i\varphi}}{h_0} = Z_R + iZ_I. \tag{1}$$

For a viscoelastic liquid of complex shear modulus $\tilde{G} = G_R + iG_I = i\omega(\eta_R - i\eta_I)$, the hydrodynamic force response in this oscillatory drainage flow, in the case of a no-slip boundary conditions at walls, is [26]

$$\tilde{Z}(D,\omega) = \frac{6\pi R^2 \tilde{G}}{D} = \frac{6\pi R^2 i\omega\tilde{\eta}}{D}. \tag{2}$$

Therefore, it is convenient to characterize the bulk viscoelasticity of the solutions by plotting $1/Z_{\text{R}}$ and $1/Z_{\text{I}}$ as a function of the sphere-plane distance, looking at large values of D (Fig. 2). At large distance, a well-defined linear behavior is observed, demonstrating the bulk viscoelastic character of the solutions. From the slope of $1/Z_R$ and $1/Z_I$, we extract the complex shear modulus components G_R and G_I.

However, contrary to the prediction of Eq. (2), the extrapolated far-field linear dependency of Z_R^{-1} and Z_I^{-1} does not point toward the distance origin but toward some negative values of D. This is usually the signature of a slippage effect at the solid-liquid interface. More specifically, it is known

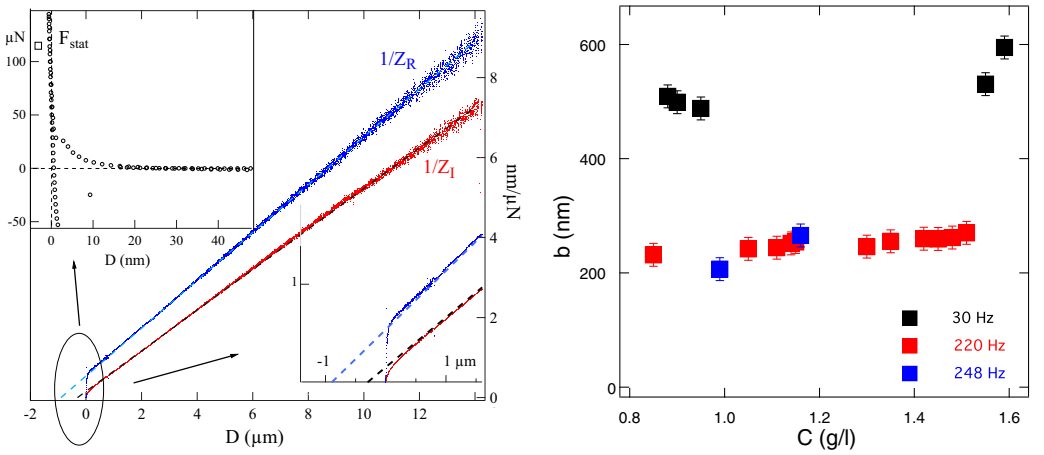

FIG. 2. Left: inverse of the components of the dynamic force response $\tilde{Z}$ measured in an HPAM solution at a frequency of 220 Hz, as a function of the sphere-plane nominal distance D. Blue, $1/Z_R$; red, $1/Z_I$. The top left inset shows the quasistatic interaction force F_{stat}, whose jump-to-contact defines the origin of distances. The bottom right inset is an enlargement at the submicrometric scale. Right: Slip length defined from the extrapolation length of $1/Z_I$ (intercept with the x axis of the black dashed line of the left plot), as a function of the concentration of the solution, for various frequencies.

in simple fluids that if a slip length b defines the slip boundary condition on each surface, then the hydrodynamic force at large distance $D \gg b$ involves the "hydrodynamic thickness" $D + 2b$ instead of the actual distance D. It is thus tempting to describe the measurements by deriving a slip length from the extrapolation lengths of $1/Z_R$ and $1/Z_I$. However, when doing so, two difficulties appear. First, the two linear extrapolations actually point toward two different origins, which is not consistent with a single, well-defined slip length. Instead, the extrapolations tend to show that the slip length is complex, possessing a real and an imaginary components. Second, if one determines the slip length as in simple liquids from the extrapolation length of the damping $1/Z_I$, one finds that it depends significantly on the frequency of the oscillatory flow (see Fig. 2). At a concentration of $\sim$1 g/L, for instance, the slip length decreases by a factor larger than 3 when the frequency increases from 30 to 220 Hz. This complex and frequency-dependant behavior of the slip length does not reflect the mechanism usually producing large slip of polymer solutions on solid surfaces, which involves the presence of an interfacial depletion layer made of pure solvent [21,22]: In the presence of a purely Newtonian lubricating layer, one should expect a purely dissipative and fully Newtonian friction mechanism of the polymer solution onto the solid surface.

These two difficulties arise because the slip length b is actually defined as the ratio η/λ of the liquid viscosity to the interfacial friction coefficient first introduced by Navier in his original statement of the boundary condition [14]:

$$\lambda v_{\text{slip}} = \eta \frac{\partial v(z)}{\partial z}. \tag{3}$$

For Newtonian fluids, the viscosity is a constant quantity, not dependant on the frequency or shear rate, and the slip length thus provides a convenient image of the interfacial friction. However, the mixture of bulk and interfacial properties entering in the slip length definition raises ambiguities when the fluid is non-Newtonian.

Keeping this in mind, we proceed to extract directly the interfacial friction coefficient from the force measurements in oscillatory drainage flow experiments. For this purpose, we calculate the hydrodynamic force exerted by the fluid drainage between the sphere and the plane, when the viscoelastic fluid undergoes the Navier's partial slip boundary condition, Eq. (3), on both surfaces.

We restrict to the linear response limit $h_0 \ll D$, in which all time variations are harmonic at the forcing frequency ω, and all time-varying quantities are characterized by their complex amplitude. In these conditions, the (amplitude of the) stress tensor in the liquid is $\tilde{\overline{\overline{\sigma}}} = \tilde{\eta}(\nabla\vec{\tilde{v}} +^T \nabla\vec{\tilde{v}}) - \delta\tilde{P}\overline{\overline{I}}$, where $\delta\tilde{P}$ is the amplitude of the dynamic pressure inducing the hydrodynamic force

$$\tilde{F}_{\rm dyn} = \int_0^\infty 2\pi r \delta\tilde{P}(r) dr. \tag{4}$$

Navier's boundary condition (3) is used with a complex friction coefficient $\tilde{\lambda}$. In a Maxwell model of the interface, $1/\tilde{\lambda} = 1/\lambda_R + i/\omega k$, where k is the interface stiffness and λ_R is the dissipative friction coefficient.

At small distance $D \ll R$, most of the hydrodynamic force originates from regions where the two solid surfaces are almost parallel. In these conditions, for angular frequencies such that $T = 2\pi/\omega \gg |\tilde{\eta}|/\rho R D$ inertia is negligible, and the average flow velocity is given by the lubrication approximation [27]:

$$\tilde{u}(r) = \frac{1}{z}\int_0^z \tilde{v}_r(r,y)dy = -\frac{1}{12\tilde{\eta}}\frac{d\delta\tilde{P}}{dr}\left(z^2 + 6z\frac{\tilde{\eta}}{\tilde{\lambda}}\right), \tag{5}$$

where $z(r)$ is the nominal gap between the surfaces at distance r from the axis. Note that the fluid velocity and the dynamic pressure $\delta\tilde{P}$ are of first order in h_0, so that only the nominal gap $z(r)$, equal to $z = D + r^2/2R$ in the parabolic approximation, enters in (5). For rigid solid surfaces, the average velocity $\tilde{u}(r)$ obeys the conservation relation:

$$\frac{d[2\pi r z(r)\tilde{u}(r)]}{dr} = -2\pi r\frac{\partial z(r)}{\partial t} = -2\pi r i\omega h_0. \tag{6}$$

Equations (5) and (6) give the following equation for the pressure:

$$\frac{d}{dr}\left[rz^2\left(z + \frac{6\tilde{\eta}}{\tilde{\lambda}}\right)\frac{d\delta\tilde{P}}{dr}\right] = 12 i\omega r\tilde{\eta}h_0, \tag{7}$$

which is integrated twice with $rdr = Rdz$ to obtain the hydrodynamic force:

$$\tilde{Z} = \frac{\tilde{F}_{\rm dyn}}{h_0} = \frac{6\pi R^2 i\omega\tilde{\eta}}{D} f^*\left(\frac{\tilde{\eta}}{\tilde{\lambda}D}\right), \tag{8}$$

$$f^*(\tilde{y}) = \frac{1}{3\tilde{y}}\left[\left(1 + \frac{1}{6\tilde{y}}\right)\ln(1 + 6\tilde{y}) - 1\right]. \tag{9}$$

Note that the logarithm entering Eq. (9) should be calculated taking into account the complex character of its argument, by $\ln(re^{i\theta}) = \ln r + i\theta$.

Equations (8) and (9) generalize the Hocking expression [27] derived for a Newtonian liquid slipping on the solid surfaces with a slip length b. In the Hocking expression, the factor f^* has the same mathematical expression as in Eq. (9), but it depends only on the simple ratio D/b. In the present non-Newtonian case, we see that a "complex slip length" $\tilde{b} = \tilde{\eta}/\tilde{\lambda}$ governs the hydrodynamic force, which explains the two extrapolation lengths observed in Fig. 2. The complex character of the slip length reflects the phase difference between the boundary slip velocity and the bulk velocity, and the ratio $\tilde{b}/D$ reflects the impact in amplitude and phase of the wall slippage in the bulk flow. We can see that for a viscoelastic liquid the slip length $\tilde{b}$ is complex even if the interfacial friction is purely dissipative, which suggests that the complex frequency-dependant slip length observed above might be only an artifact due to the bulk behavior of the solutions.

In order to disentangle experimentally the interfacial boundary condition from the bulk properties of the solutions, we notice that at large distance $D \gg |\tilde{\eta}/\tilde{\lambda}|$, the above expression (8) expands as

$$\frac{1}{\tilde{Z}} = \frac{D}{6\pi R^2 i\omega\tilde{\eta}} + \frac{1}{3\pi i\omega R^2\tilde{\lambda}}. \tag{10}$$

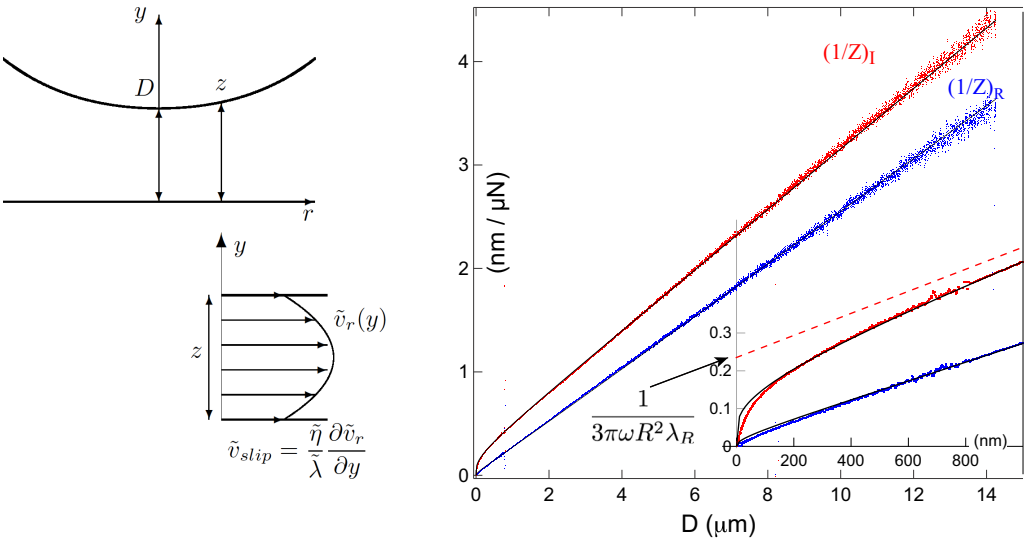

FIG. 3. Left: schematic of the sphere-plane geometry and of the flow profile. Right: elastic component $(1/\tilde{Z})_R$ (blue dots) and dissipative component $(1/\tilde{Z})_I$ (red dots) of the inverse of the force response measured in an HPAM solution at a frequency of 220 Hz. The black continuous lines are the components of the theoretical expression (8) fitted with a real-valued boundary friction coefficient $\tilde{\lambda} = \lambda_R$. Inset: enlargement below the micrometric scale. The red dashed line is the extrapolation of the far-field behavior of $(1/\tilde{Z})_I$.

Thus, rather than Z_R^{-1} and Z_I^{-1}, the dynamic quantity providing an independent access to the interfacial rheology is $1/\tilde{Z}$. More specifically, the boundary friction and stiffness are obtained from the value at origin (intercept on the y axis) of the linear extrapolation of the far-field components $(1/\tilde{Z})_R$ and $(1/\tilde{Z})_I$. Accordingly, the components of $1/\tilde{Z}$ in our HPAM solutions are plotted in Fig. 3. The linear extrapolation of $(1/\tilde{Z})_R$ points toward the origin within the experimental resolution. This shows that elastic effects in the interface response are negligible: $k \simeq 0$ and $\tilde{\lambda}$ reduces to λ_R. The purely dissipative nature of the interfacial friction coefficient reflects the physical mechanism inducing the apparent slip, i.e., the lubrication effect of a Newtonian liquid layer at the boundary.

The linear extrapolation of $(1/\tilde{Z})_I$ (dashed red line in Fig. 3) does not extrapolate to zero and gives a first estimation of the liquid-solid friction coefficient λ_R, in the range of 30 μPa s/nm. For a precise determination of λ_R, it is, however, important to compare the whole data to the theoretical expression (8) and (9), because the asymptotic linear dependency of $1/\tilde{Z}$ with D is reached only at very large distances $D \gg |\tilde{\eta}|/|\lambda|$. At smaller distances, $(1/\tilde{Z})_I$ curves down continuously, converging finally toward the physical origin. This tendency is in excellent agreement with our theory which provides a very accurate prediction of both components of the measured dynamic force (see Fig. 3).

Precise estimations of the boundary friction coefficient λ_R are obtained for various concentrations and frequencies by fitting the data to Eqs. (8) and (9) and are plotted in Fig. 4. Unlike the slip length (Fig. 2), the friction coefficient is essentially insensitive to the frequency over the range studied, which extends over 1 decade. The absence of frequency evolution is the signature of a fully Newtonian interfacial friction, as expected for a slippage mechanism involving a fully depleted, pure water layer at the solution-solid interface. In contrast, the viscoelastic modulii of the solutions vary significantly in the range of frequencies studied (see Fig. 4 left). This variation accounts fully for the frequency dependance of the slip length measured in Fig. 2, which is thus due to the bulk rheology of the solutions and not to the boundary hydrodynamics. Assuming that the viscosity of the depletion layer is that of pure water, its estimated thickness $e_s \simeq \eta_{\text{water}}/\lambda$ [28,29] varies between 40 and 26 nm for a bulk concentration of polymer between 0.8 and 1.6 g/L. Furthermore, we should emphasize that in dynamic SFA experiments, the wall shear rate is not spatially uniform, and its range of values

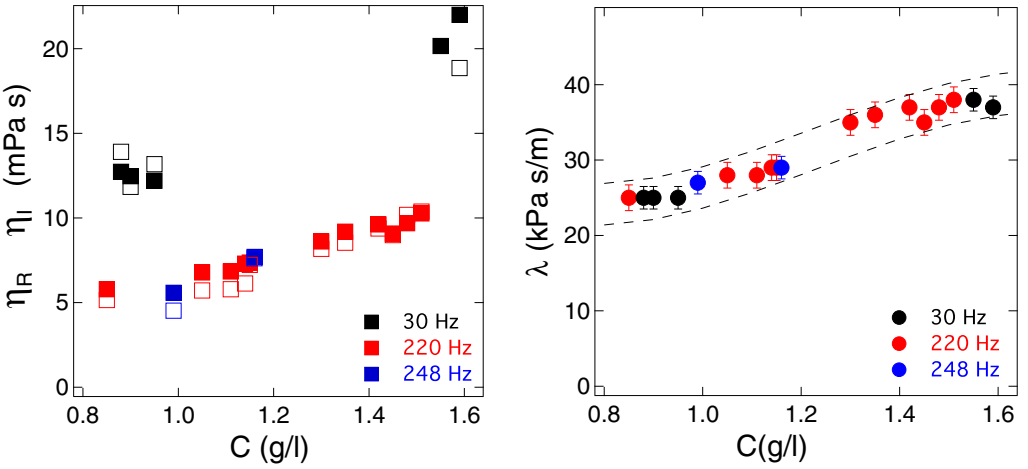

FIG. 4. Left: components η_R (■) and η_I (□) of the viscoelastic modulus $\tilde{\eta}$ of the solutions as a function of polymer concentration, at 30 Hz (black), 220 Hz (red), and 248 Hz (blue). Right: interfacial friction coefficient $\tilde{\lambda} = \lambda_R$ at the solution-solid boundary as a function of the HPAM concentration, at 30 Hz (black), 220 Hz (red), and 248 Hz (blue). The dashed lines are a guide for the eye.

changes when the nominal distance D is varied. Considering the excellent agreement of our analytical expression with the data, we can state that the boundary friction coefficient is insensitive to the flow geometry, frequency, and shear rate at wall in the range of 10^{-5} to 10^{-2} s^{-1} probed in the experiment. This shows that the boundary layer inducing the apparent slip is a purely equilibrium layer, whose properties are independent of the applied flow in the range of the above frequencies and shear rates. Such a conclusion cannot be obtained from the properties of the slip length alone, which provides a further proof that the liquid-solid friction coefficient is more appropriate than the slip length to characterize the boundary slip of a complex fluid.

Finally, we discuss the limitations at the microscopic scale of the model of apparent slip boundary condition. The connection of the macroscopic scale to the microscopic scale is shown in Fig. 5. Three areas appear on this figure. Below 20 nm, the depletion layer at the solution-solid interfaces is evidenced by the behavior of the damping $(1/\tilde{Z})_I$: The latter cannot be distinguished from a Newtonian liquid of viscosity 0.85 mPa s, essentially equal to that of water at the experiment temperature (28 °C), flowing with a no-slip boundary condition on the solid surfaces (green dashed line in Fig. 5). The microscopic scale of 20 nm is indeed in good agreement with the estimated thickness $e_s \simeq 28$ nm of the depletion layer at this polymer concentration of 1.4 g/L. Thus, at distances D smaller than e_s, the sphere-plane gap is largely filled with pure water and the hydrodynamic force resumes to the Reynolds force with a no-slip boundary condition located onto the solid surfaces. Second, at intermediate distances $e_s < D < 10\, e_s$, the polymer solution flows on a lubricating layer whose thickness cannot be neglected. Accordingly, as shown theoretically [7], the apparent b.c. has to be properly described by two independent parameters: the location of the b.c. and the interfacial friction coefficient. For a sharp and large-viscosity gradient, the appropriate apparent b.c. location lies close to the middle of the depletion layer e_s as sketched in Fig. 5. Taking this location for the b.c. instead of the actual position of the solid surfaces amounts to replacing D by $D + e_s$ in Eqs. (8) and (9). We find that it provides a significantly better agreement with the data (dashed black lines in Fig. 5). Third, at large distances $D > 10\, e_s$, the finite thickness of the depletion layer can be neglected and one retrieves the apparent slip boundary condition characterized by a friction coefficient $\tilde{\lambda} \approx \lambda_R = \eta_{\text{water}}/e_s$.

In conclusion, we have shown that the slip behavior of a complex fluid at a solid boundary should be consistently analyzed using a boundary friction coefficient rather than a slip length, in order

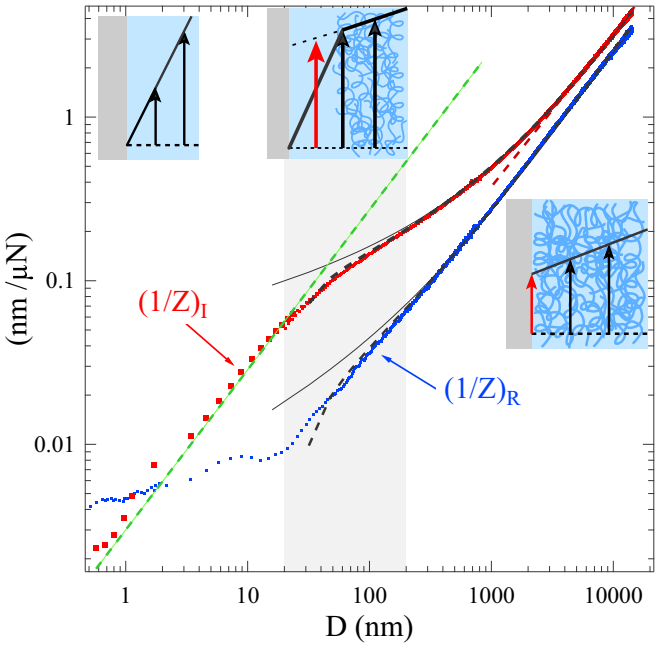

FIG. 5. Log-log plot of the components of $1/\tilde{Z}$ (blue dots, real; red dots, imaginary) in a solution of 1.4 g/L at 220 Hz, showing the macro-micro transition. The dashed red (resp. green) line corresponds to a Newtonian fluid (resp. water) with a no-slip b.c. at the solid wall. The black continuous lines are the components of the theoretical expression (8) taking into account the bulk viscoelasticity and a Navier's b.c. with a real-valued friction coefficient λ_R. The dashed continuous lines are Eq. (8) with the boundary condition applied inside the liquid, at a distance $e_s/2 = \eta_{\text{water}}/2\lambda_R = 14$ nm of each solid surface.

to account faithfully for interfacial rheology effects. In the studied case, the friction coefficient is real-valued and fully Newtonian while the slip length $\tilde{\eta}/\lambda$ is complex and frequency dependent, due to the complex bulk rheology of the solutions. This fully Newtonian friction reflects a slip mechanism due to a depletion layer made of pure solvent at the solid-polymer solution interface. Our experiments and analysis show that, beyond a proper description of the boundary condition, the friction coefficient is the relevant quantity for understanding the physical mechanisms governing the interfacial dynamics. From a fundamental point of view, the coupling between the generalized lubrication theory developed here and the unique capabilities of the SFA opens the route to develop a complete surface rheology for the solid-liquid interface that could be equivalent to what has been recently developed for the fluid-fluid interface [30]. In particular, it would be interesting to perform experiments on interfaces specifically tailored at the molecular level to provide a non-Newtonian surface friction. Polymer systems are choice candidates to do so.

This research was supported by the Agence Nationale pour la Recherche program ANR-15-CE06-0005.

[1] H. A. Barnes, A review of the slip (wall depletion) of polymer solutions, emulsions, and particle suspensions in viscositmer: Its cause, character, and curve, J. Non-Newtonian Fluid Mech. **56**, 221 (1995).
[2] M. M. Denn, Extrusion instability and wall slip, Annu. Rev. Fluid Mech. **33**, 265 (2001).

[3] G. Reiter and R. Khanna, Real-Time Determination of the Slippage Length in Autophobic Polymer Dewetting, Phys. Rev. Lett. **85**, 2753 (2000).
[4] O. Baumchen and K. Jacobs, Slip effects in polymer thin films, J. Phys.: Condens. Matter **22**, 033102 (2010).
[5] S. G. Hatzikiriakos, Wall slip in molten polymers, Prog. Polym. Sci. **37**, 624 (2012).
[6] P. A. Thompson and M. O. Robbins, Shear flow near solids: Epitaxial order and flow boundary conditions, Phys. Rev. A **41**, 6830 (1990).
[7] L. Bocquet and J.-L. Barrat, Hydrodynamic boundary conditions, correlation functions, and Kubo relations for confined fluids, Phys. Rev. E **49**, 3079 (1994).
[8] P. A. Thompson and S. M. Troian, A general boundary condition for liquid flows at solid surfaces, Nature (London) **389**, 360 (1997).
[9] R. Pit, H. Hervet, and L. Léger, Direct Experimental Evidence of Slip in Hexadecane: Solid Interfaces, Phys. Rev. Lett. **85**, 980 (2000).
[10] L. Thomas, E. Charrault, and C. Neto, Interfacial slip on rough, patterned, and soft surfaces: A review of experiments and simulations, Adv. Colloid Interface Sci. **210**, 21 (2014).
[11] E. Secchi, S. Marbach, A. Niguès, D. Stein, A. Siria, and L. Bocquet, Massive radius-dependent flow slippage in carbon nanotubes, Nature (London) **537**, 210 (2016).
[12] S. Leroy, A. Steinberger, C. Cottin-Bizonne, F. Restagno, L. Léger, and E. Charlaix, Hydrodynamic Interaction Between a Spherical Particle and An Elastic Surface: A Gentle Probe for Soft Thin Films, Phys. Rev. Lett. **108**, 264501 (2012).
[13] M. Hénot, A. Chennevière, E. Drockenmuller, L. Léger, and F. Restagno, Comparison of the slip of a PDMS melt on weakly adsorbing surfaces measured by a new photobleaching-based technique, Macromolecules **50**, 5592 (2017).
[14] C. L. Navier, Mémoires sur les lois du mouvement des fluides, Mem. Acad. Sci. Inst. France **6**, 389 (1823).
[15] A. V. Dobrynin and M. Rubinstein, Theory of polyelectrolytes in solutions and at surfaces, Prog. Polym. Sci. **30**, 1049 (2005).
[16] G. Chauveteau, M. Tirrell, and A. Omari, Concentration dependence of the effective viscosity of polymer solutions in small pores with repulsive or attractive walls, J. Colloid Interface Sci. **100**, 41 (1984).
[17] A. Omari, M. Moan, and G. Chauveteau, Wall effect in the flow of flexible polymer solution through small pores, Rheol. Acta **28**, 520 (1989).
[18] J. Cayer-Barrioz, D. Mazuyer, A. Tonck, and E. Yamaguchi, Drainage of a wetting liquid: Effective slippage or polymer depletion? Tribo. Lett. **32**, 81 (2008).
[19] A. Cuenca and H. Bodiguel, Submicron Flow of Polymer Solutions: Slippage Reduction Due To Confinement, Phys. Rev. Lett. **110**, 108304 (2013).
[20] P. G. De Gennes, Polymer solutions near an interface. adsorption and depletion layers, Macromolecules **14**, 1637 (1981).
[21] T. L. Kuhl, A. D. Berman, S. W. Hui, and J. N. Israelachvili, Part 1. Direct measurement of depletion attraction and thin film viscosity between lipid bilayers in aqueous polyethylene glycol solutions, Macromolecules **31**, 8250 (1998).
[22] R. G. Horn, O. I. Vinogradova, M. E. Mackay, and N. Phan-Thien, Hydrodynamic slippage inferred from thin film drainage measurements in a solution of nonadsorbing polymer, J. Chem. Phys. **112**, 6424 (2000).
[23] W. Knoben, N. A. M. Besseling, and M. A. Cohen Stuart, Direct measurement of depletion and hydrodynamic forces in solutions of a reversible supramolecular polymer, Langmuir **23**, 6095 (2007).
[24] F. Restagno, J. Crassous, E. Charlaix, C. Cottin-Bizonne, and M. Monchanin, A highly sensitive dynamic surface force apparatus for nanorheology, Rev. Sci. Instrum. **73**, 2292 (2002).
[25] L. Garcia, C. Barraud, C. Picard, J. Giraud, E. Charlaix, and B. Cross, A micro-nano-rheometer for the mechanics of soft matter at interfaces, Rev. Sci. Instrum. **87**, 113906 (2016).
[26] E. Pelletier, J.-P. Montfort, and F. Lapique, Surface force apparatus and its application to nanorheological studies, J. Rheol. **38**, 1151 (1994).
[27] L. M. Hocking, The effect of slip on the motion of a sphere close to a wall and of two adjacent spheres, J. Eng. Math. **7**, 207 (1973).

[28] O. I. Vinogradova, Drainage of a thin liquid film confined between hydrophobic surfaces, Langmuir **11**, 2213 (1995).
[29] R. Tuinier and T. Taniguchi, Polymer depletion-induced slip near an interface, J. Phys.: Condens. Matter **17**, L9 (2005).
[30] M. Brenner and S. Howard, *Interfacial Transport Processes and Rheology* (Elsevier, Amsterdam, 2013).